In utero MRI identifies consequences of early-gestation alcohol drinking on fetal brain development in rhesus macaques

Xiaojie Wang[a,b], Verginia C. Cuzon Carlson[a,c], Colin Studholme[d,e,f], Natali Newman[a], Matthew M. Ford[a], Kathleen A. Grant[a,c], and Christopher D. Kroenke[a,b,c,1]

[a]Division of Neuroscience, Oregon National Primate Research Center, Oregon Health & Science University, Beaverton, OR 97006; [b]Advanced Imaging Research Center, Oregon Health & Science University, Portland, OR 97214; [c]Department of Behavioral Neuroscience, Oregon Health & Science University, Portland, OR 97239; [d]Biomedical Image Computing Group, Department of Pediatrics, University of Washington, Seattle, WA 98105; [e]Department of Bioengineering, University of Washington, Seattle, WA 98105; and [f]Department of Radiology, University of Washington, Seattle, WA 98105

Edited by Pasko Rakic, Yale University, New Haven, CT, and approved March 20, 2020 (received for review November 15, 2019)

One factor that contributes to the high prevalence of fetal alcohol spectrum disorder (FASD) is binge-like consumption of alcohol before pregnancy awareness. It is known that treatments are more effective with early recognition of FASD. Recent advances in retrospective motion correction for the reconstruction of three-dimensional (3D) fetal brain MRI have led to significant improvements in the quality and resolution of anatomical and diffusion MRI of the fetal brain. Here, a rhesus macaque model of FASD, involving oral self-administration of 1.5 g/kg ethanol per day beginning prior to pregnancy and extending through the first 60 d of a 168-d gestational term, was utilized to determine whether fetal MRI could detect alcohol-induced abnormalities in brain development. This approach revealed differences between ethanol-exposed and control fetuses at gestation day 135 (G135), but not G110 or G85. At G135, ethanol-exposed fetuses had reduced brainstem and cerebellum volume and water diffusion anisotropy in several white matter tracts, compared to controls. Ex vivo electrophysiological recordings performed on fetal brain tissue obtained immediately following MRI demonstrated that the structural abnormalities observed at G135 are of functional significance. Specifically, spontaneous excitatory postsynaptic current amplitudes measured from individual neurons in the primary somatosensory cortex and putamen strongly correlated with diffusion anisotropy in the white matter tracts that connect these structures. These findings demonstrate that exposure to ethanol early in gestation perturbs development of brain regions associated with motor control in a manner that is detectable with fetal MRI.

FASD | nonhuman primate | diffusion MRI | cerebellum | white matter

Exposure to alcohol during fetal development is associated with anatomical abnormalities in the developing central nervous system (CNS) and adverse functional deficits, such as behavioral and cognitive impairments. Collectively, these are termed fetal alcohol spectrum disorders (FASD), which remains a highly prevalent neurodevelopmental disorder in the United States and worldwide (1). Despite public recognition of the teratogenic nature of alcohol, the prevalence of FASD is still estimated to be as high as 1.1 to 5.0% among school-age children in the United States (2–4). Although most women will completely stop or reduce the amount of alcohol consumed after pregnancy awareness, the rate of unplanned pregnancies (45%) (5), combined with alcohol drinking in 56% of reproductive age women (6), results in an estimated 11.5% and 3.9% of pregnancies in which alcohol drinking or binge drinking occurred, respectively (7). Early diagnosis of FASD is critical. This is substantiated by the observation that the odds ratios of several adverse life outcomes decrease when therapeutic intervention strategies are initiated early in life (8, 9). Recent advances in magnetic resonance image (MRI) reconstruction techniques (10–12) have enabled high-resolution anatomical and diffusion MRI measurements to be performed on the fetal brain in utero. These are powerful noninvasive tools to quantify macroscopic (13–15) and microscopic (16–19) aspects of fetal brain development. If fetal MRI could be demonstrated to be sufficiently sensitive to detect alcohol-induced developmental abnormalities, it could provide a new strategy for addressing this prevalent disorder.

We recently developed a rhesus macaque model of early-pregnancy drinking (20). The neurodevelopmental events that occur during gestational development in rhesus macaques resemble those of humans more closely than do other animal model species (21), which presents the opportunity to assess the capabilities of fetal MRI for observing alcohol-induced effects in CNS development. In this study, female rhesus macaques that drank 1.5 g/kg of ethanol daily, beginning prior to pregnancy and extending through the first 60 d of a 168-d gestational term, underwent fetal MRI procedures at gestational ages (G)85, G110, or G135 (Fig. 1*A*). Fetuses of ethanol-drinking dams were compared to control age-matched fetuses of dams who drank an isocaloric maltose-dextrin solution. Fetal brain development was characterized with T_2-weighted and diffusion MRI. In order to

Significance

Early diagnosis of fetal alcohol spectrum disorder (FASD) is necessary for initiating early therapy, and is the most effective way to reduce risk of long-term adverse outcomes. This study utilized a nonhuman primate model of FASD, and is the first to exploit in utero MRI to detect the effects of early-pregnancy drinking on the fetal brain. Alterations in motor-related brain regions become detectable with in utero MRI at the beginning of the third-trimester equivalent in human pregnancy. Follow-up electrophysiological measurements demonstrated that the MRI-identified brain abnormalities are associated with aberrant brain function. These findings demonstrate the sensitivity of in utero MRI, and inform future clinical studies on the timing and brain region of greatest sensitivity to early ethanol exposure.

Author contributions: X.W., V.C.C.C., K.A.G., and C.D.K. designed research; X.W., V.C.C.C., C.S., N.N., M.M.F., K.A.G., and C.D.K. performed research; X.W., V.C.C.C., C.S., M.M.F., K.A.G., and C.D.K. contributed new reagents/analytic tools; X.W., V.C.C.C., C.S., K.A.G., and C.D.K. analyzed data; and X.W., V.C.C.C., and C.D.K. wrote the paper.

The authors declare no competing interest.

This article is a PNAS Direct Submission.

Data deposition: MRI-derived parameters and electrophysiological results obtained as part of this study are available through the Monkey Alcohol Tissue Research Resource https://gleek.ecs.baylor.edu/static/publication_data/FAS_Cohort_MRI_Ephys_Data_Wang_et_at_2020.xlsx.

[1]To whom correspondence may be addressed. Email: kroenkec@ohsu.edu.

This article contains supporting information online at https://www.pnas.org/lookup/suppl/doi:10.1073/pnas.1919048117/-/DCSupplemental.

avoid confounds associated with repeated exposure to anesthesia, this study employed a cross-sectional design, such that MRI was conducted only once per animal. This experiment therefore facilitated comparisons between alcohol-exposed and control fetuses over a range of gestational ages to determine the most sensitive stage of gestation for detecting differences. In order to characterize the potential functional significance of anatomical abnormalities revealed by MRI, ex vivo electrophysiological recordings were performed on fetal brain tissue immediately following MRI examination.

Results

Generation of the 28 fetuses (14 ethanol and 14 controls) used in this study is detailed in ref. 20. Pregnancies were detected between G30 and G50 with ultrasound performed on awake dams, and all confirmed pregnancies reached the planned experimental time point of G85, G110, or G135. One fetus from the control group was from a dam with a spontaneously occurring case of placental insufficiency, leading to intrauterine growth restriction (22), and was excluded from further analysis as a result. The distribution of numbers for the remaining animals across each gestational time point is shown in Fig. 1*A*. In addition, one fetus (fetal ID F10289, as described in the Monkey Alcohol Tissue Research Resource [MATRR] website, https://gleek.ecs.baylor.edu/) in the G135 group was exposed to ethanol through the first 108, rather than 60 d of gestation (20). Measurements performed on this fetus are highlighted as open symbols in Figs. 2–4. Given that outcome measures from this fetus are typical for the G135 ethanol-exposed group, it is included in the statistical analyses performed herein. Fetal tissues have been deposited to the MATRR (https://gleek.ecs.baylor.edu/). Detailed information regarding maternal blood ethanol concentration (BEC), fetal sex, and birth weight have been summarized in Jimenez et al. (20).

Effects of Early-Gestation Alcohol on Fetal Brain Size. Gross anatomical brain abnormalities were observed in one fetus (F10283) from the G110 cohort (Fig. 1*B*) and one fetus (F10290) from the G135 cohort (Fig. 1*C*). In both cases, the lateral ventricles were substantially enlarged, compared to control fetuses at the corresponding gestational age, as apparent in T_2-weighted images (Fig. 1 *B* and *C*, red arrowheads). This anomaly was not present in any of the control fetal brains over the gestational age range examined (*SI Appendix*, Figs. S1–S3).

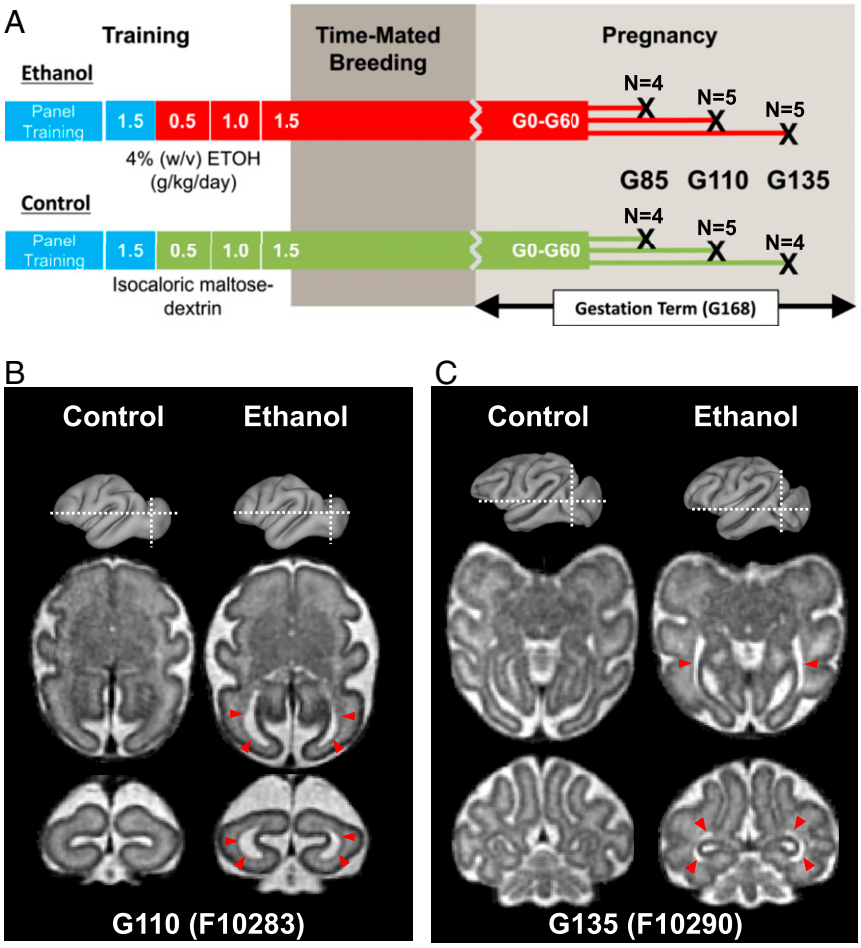

Fig. 1. Experimental timeline and gross findings. (*A*) Female rhesus macaques were assigned to either an ethanol (*Upper*) or a control (*Lower*) groups. Animals were induced to drink a 4% ethanol solution or a caloric equivalent maltose dextrin solution over a 120-d induction period, starting with 0.5, followed by 1.0, and then finally 1.5 g/kg per day (blue bars indicate water-drinking phases, red bars indicate ethanol-drinking phases, and green bars indicate maltose dextrin-drinking phases of the experiment). In the ethanol group, each pregnant female maintained daily voluntary intake of 1.5 g/kg until G60. At G85, G110, and G135 dams underwent in vivo MRI. The numbers of fetuses for each group and time point are indicated. Modified with permission from ref. 20. (*B* and *C*) Two ethanol-exposed fetuses, one from the G110 cohort (*B*) and one from the G135 cohort (*C*), were found to have enlarged lateral ventricles compared to age-matched controls. This is evident on axial and coronal T_2-weighted images (red arrowheads) at marked locations (white dashed lines on gray 3D surface). Representative fetal brains from the G110 and G135 control groups are also shown for comparison.

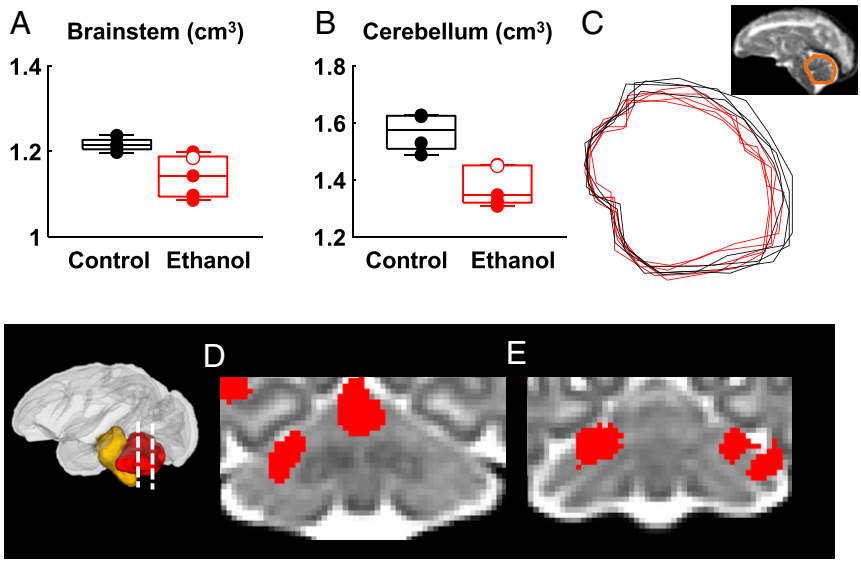

Fig. 2. Fetal ethanol exposure is associated with brainstem and cerebellum volume reduction, observable at G135. (*A*) Brainstem volumes are smaller in the ethanol group (corrected $P = 0.046$) compared to that of control. (*B*) Cerebellar volumes are smaller in the ethanol group (corrected $P = 0.020$) relative to control. (*C*) Midsagittal traces of the cerebellum for the G135 ethanol group (red) and control group (black). Tensor-based morphometry revealed that all clusters of local volume differences that overlapped cerebellum reflected regions where the ethanol-exposed cerebellum is smaller than the gestation-matched control. Clusters with uncorrected $P \leq 0.05$ and size ≥ 125 mm^3 were shown in red and overlaid on the study-specific template. (*D*) One cluster overlaps the cerebellar vermis (*E*) and additional bilateral clusters overlap lobule VI and Crus I. Black symbols: control fetuses; red symbols: ethanol-exposed fetuses; red open symbol: fetus F10289 who was exposed to 108 d of ethanol drinking.

NEUROSCIENCE

In order to compare overall brain sizes, age-appropriate rhesus macaque template images were used, which have each been segmented into a common set of six brain regions (23). The total brain volume and the volumes of each brain region were determined following nonlinear registration of the segmented template to each fetus' T_2-weighted image. At G85 and G110, no differences were found between any of the brain regional volumes (*SI Appendix*, Tables S1 and S2) However, in the G135 brains, reduced cerebellar (corrected $P = 0.020$) and brainstem (corrected $P = 0.046$) volumes are observed in the ethanol-exposed animals compared to controls (Fig. 2 and Table 1). In addition to the analyses of brain region volumes, global measures of brain structure were also compared. Total brain volume does not differ between the control and ethanol-exposed fetuses ($P > 0.05$) at any of the three gestational ages. Taking these data together, this analysis indicates the G135 cerebellum and brainstem exhibit heightened sensitivity to early gestation ethanol exposure compared to other brain regions and developmental stages.

Previous neuroimaging studies of children exposed to fetal alcohol have demonstrated heightened vulnerability of the anterior vermis (24, 25) compared to other regions of the cerebellum. Evidence of vermal hypoplasia in the ethanol-exposed G135 fetuses is shown in traces of the cerebellar midline for controls and ethanol-exposed animals (black and red traces in Fig. 2*C*, respectively), in which the latter is consistently smaller. To further explore regional variation in shape, after adjusting for variation in overall brain size, tensor-based morphometry was performed on the G135 brains. Log-transformed determinants of the Jacobian maps of warp-fields that transform the individual brains to an age-specific template were analyzed to determine clusters in which control brain regions were larger than corresponding ethanol-exposed brain regions, and vice versa. All clusters of local volume differences that overlapped the cerebellum reflected regions where the ethanol-exposed cerebellum is smaller than the gestation-matched control (i.e., no clusters of locally enlarged volumes were observed for ethanol-exposed brains in the cerebellum). As shown in Fig. 2*D*, one cluster overlapped the anterior vermis. Fig. 2 *D* and *E* illustrate additional bilateral clusters that overlap lobule VI and Crus I. In the brainstem, no cluster of locally contracted regions associated with ethanol exposure was detected, indicating the reductions in the sizes of ethanol-exposed brainstems are homogeneously distributed throughout this structure.

Effects of Early-Gestation Alcohol on White Matter Development. Previous studies of children affected by FASD have identified abnormalities in white matter fractional anisotropy (FA), which indicates that alcohol exposure interferes with structural development of myelinated white matter tracts (26–36). In order to address whether water-diffusion measurements could be used to detect abnormal maturation in the developing fetal brain, FA was compared between ethanol-exposed and control fetuses. In a previous study of normally developing rhesus macaque fetal brains, regions of interest (ROIs) were delineated on 8 white matter fiber systems at G110 and 11 fibers at G135 (23). These ROIs were propagated to the reference frames for FA of each individual fetus, and the average value within the ROI was determined. In five white matter bundles (the anterior limb of the internal capsule [ALIC], posterior limb of the internal capsule

Table 1. Comparison of brain region volumes between control and ethanol-exposed fetuses at G135

	Control (cm^3)	Ethanol (cm^3)	Corrected *P*
Cortical plate	16.40 ± 1.04	15.78 ± 0.37	0.14
White matter	14.79 ± 1.08	14.03 ± 0.85	0.15
Striatum	1.27 ± 0.10	1.22 ± 0.07	0.20
Thalamus	1.15 ± 0.05	1.08 ± 0.05	0.064
Brainstem	**1.22 ± 0.02**	**1.14 ± 0.05**	**0.046**
Cerebellum	**1.57 ± 0.07**	**1.38 ± 0.07**	**0.020**
Whole brain	37.11 ± 2.0	35.39 ± 1.0	0.090

Brain region volumes (group mean ± group SD). Corrected *P* values reflect two-sample, one-tailed (control > ethanol) *t* tests, controlled for false-discovery rate using the BH procedure (bold, corrected $P < 0.05$).

[PLIC], corticospinal tract [CST], superior cerebellar peduncle [SCP], and middle cerebellar peduncle [MCP]) at G135, FA was found to be smaller in ethanol-exposed fetuses compared to controls (Fig. 3 and Table 2). No differences in FA were observed at G110 (*SI Appendix*, Table S3). Notably, the set of white matter fibers affected by early gestation ethanol exposure primarily involved axons that contribute to motor circuitry, which involves the cerebellar and brainstem structures that exhibit affected volume in ethanol-exposed G135 fetuses.

In order to characterize the pattern of affected white matter in greater detail, a voxel-wise analysis was performed to compare FA maps from the control and the ethanol groups at G135. In line with the findings from ROI-based comparisons, the ALIC and PLIC (Fig. 3*G*, blue arrowheads), CST (Fig. 3 *I* and *N*, green arrowheads), SCP (Fig. 3*J*, cyan arrowheads), and MCP (Fig. 3 *H*, *J*, and *N*, magenta arrowheads) of ethanol-exposed fetuses show extensive reductions in FA compared to those of controls. In addition, regions within the corpus callosum (CC) (Fig. 3 *G* and *M*), uncinate fasciculus (Fig. 3 *G* and *L*, blue arrows), and corona radiata (Fig. 3 *K* and *L*, green arrows) also show reduced FA in ethanol-exposed fetuses compared to controls. Similar voxel-wise analyses of the G85 and G110 cohorts did not reveal white matter regions that differed in diffusion anisotropy between ethanol-exposed and control groups.

Although each ethanol-drinking animal in this study consumed the same daily dose (1.5 g/kg/d) over the first 60 d of gestation, individual differences in the BEC values achieved by each monkey were observed, due to differences in the rates of ethanol intake (20). It was therefore of interest to determine whether the extent of fetal brain maturation outcomes were associated with

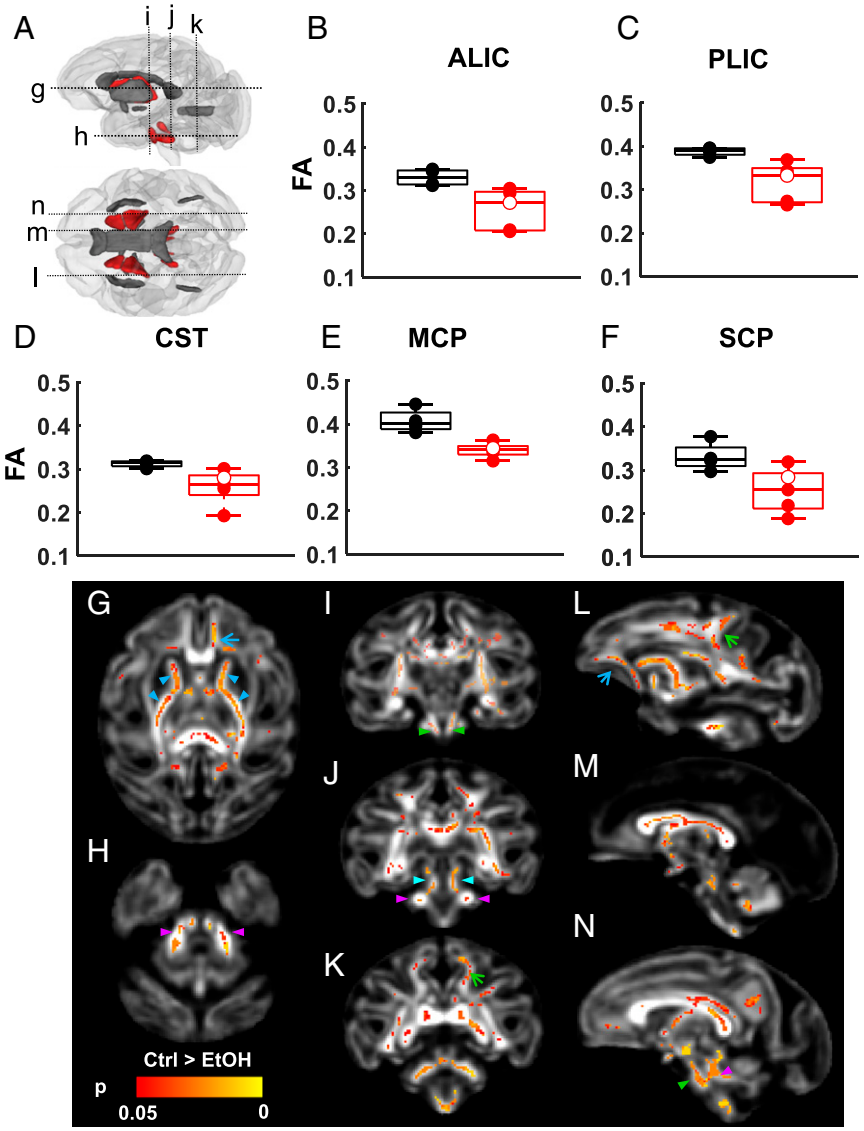

Fig. 3. Lower white matter FA at G135 is associated with fetal ethanol exposure. (*A*) For the 11 white matter tracts (red and gray ROIs) characterized at G135, 5 were found to have reduced FA associated with fetal ethanol exposure (red ROIs). (*B*) Anterior (ALIC, corrected $P = 0.046$) and (*C*) posterior (PLIC, corrected $P = 0.046$) limbs of the internal capsule, (*D*) the CST ($P = 0.047$), (*E*) the MCP ($P = 0.020$), and (*F*) the SCP (corrected $P = 0.047$) show significantly lower FA than those of age-matched controls. Black symbols: control fetuses; red symbols: ethanol-exposed fetuses; red open symbol: fetus F10289 who was exposed to 108 d of ethanol drinking. (*G–N*) TBSS was also performed on FA maps of these fetal brains to characterize FA differences at a voxel level. Internal capsule (*G*, blue arrowheads), CST (*I* and *N*, green arrowheads), MCP (*H*, *J*, and *I*, magenta arrowheads), and SCP (*J*, cyan arrowheads) show extensive reduction in FA compared to that of control. In addition, regions within the CC (*M* and *N*), uncinate fasciculus (*G* and *L*, blue arrows), and corona radiata (*K* and *L*, green arrows) also show reduction in FA in the ethanol-exposed fetuses compared to that of control fetuses.

Table 2. Comparison of white matter FA between control and ethanol-exposed fetuses at G135

ROI	Control	Ethanol	Corrected *P*
CC	0.54 ± 0.04	0.42 ± 0.09	0.061
AC	0.33 ± 0.04	0.27 ± 0.05	0.094
ALIC	**0.33 ± 0.02**	**0.26 ± 0.05**	**0.046**
PLIC	**0.39 ± 0.01**	**0.32 ± 0.04**	**0.046**
Fornix	0.39 ± 0.04	0.34 ± 0.02	0.061
CST	**0.31 ± 0.01**	**0.26 ± 0.04**	**0.047**
SCP	**0.33 ± 0.03**	**0.25 ± 0.05**	**0.047**
MCP	**0.41 ± 0.03**	**0.34 ± 0.02**	**0.020**
EC	0.21 ± 0.01	0.18 ± 0.03	0.067
PTR	0.32 ± 0.03	0.27 ± 0.04	0.094
Cereb.Ped.	0.33 ± 0.01	0.27 ± 0.06	0.061

FA values (group mean ± group SD). Corrected *P* values are from two-sample, one-tailed (control > ethanol) *t* tests, controlled for false-discovery rate using the BH procedure. EC, external capsule (bold, corrected $P < 0.05$).

maternal BEC. Pearson correlation coefficients between the average BEC over the first 60 d of gestation, and each of the MRI-derived metrics (*SI Appendix*, Tables S4–S6), yielded statistically significant correlation values ($P < 0.05$) only within G135 brains, where brainstem and thalamic volume—as well as FA within the CC, ALIC, PLIC, CST, and SCP—were negatively correlated with maternal BEC (*SI Appendix*, Table S6). These correlations are restricted to brain regions that exhibit marked group differences between ethanol-exposed and control fetuses, albeit only at trend level for the thalamic volume ($P = 0.064$) (Table 1) and FA in the CC ($P = 0.061$) (Table 2). Moreover, significant correlations with BEC were not observed for any of these structures exclusively within the ethanol-exposed group. It is likely, therefore, that the observed correlations with BEC are consequences of group differences between ethanol-exposed and control fetuses, rather than proportional effects within the limited range of variability in BEC values among the G135 animals.

Associations between Anatomical and Functional Consequences of Fetal Ethanol on Brain Development. In order to validate that the anatomical abnormalities observed in ethanol-exposed fetuses were of functional significance, ex vivo whole-cell patch-clamp electrophysiological recordings were performed immediately following the acquisition of MRI data. Due to the high prevalence of sensory-motor deficits and frequently reported structural and functional alternations in the striatum in the human FASD population, combined with results from mouse studies demonstrating electrophysiological effects of early gestation ethanol exposure on neurons located within the primary somatosensory cortex (SS) (37) and the striatum (38), the SS (Fig. 4*A*, blue ROI), the putamen (Fig. 4*A*, maroon ROI), and the caudate (Fig. 4*A*, orange ROI) were targeted for electrophysiological recordings of spontaneous excitatory and inhibitory postsynaptic currents (sEPSCs and sIPSCs, respectively) (Fig. 4*B*). The characteristics of current frequency and amplitude were compared to the MRI data. All of the white matter structures that exhibited ethanol exposure-related reductions in FA in G135 brains (the ALIC, PLIC, CST, SCP, and MCP) also exhibited statistically significant correlations with sEPSC amplitude in the SS, and three structures (the ALIC, PLIC, and MCP) were correlated with sEPSC amplitude in the putamen (Fig. 4 and Table 3). Diffusion anisotropy was also correlated with sEPSC amplitude in structures that were not significantly different between ethanol-exposed and control G135 fetuses. Specifically, the CC, anterior commissure (AC), and cerebral peduncle (Cereb Ped) are significantly positively correlated with sEPSC amplitude recorded from pyramidal neurons within the SS, and FA within the AC, posterior thalamic radiation (PTR), and Cereb Ped correlated with the ESPC amplitude of medium spiny neurons recorded within the putamen (Table 3). No statistically significant correlations were observed between diffusion anisotropy and sEPSC frequency (*SI Appendix*, Table S7), nor sIPSCs frequency or amplitude (*SI Appendix*, Tables S8 and S9, respectively). In contrast to the putamen and SS, no electrophysiological parameters measured in the caudate were observed to be correlated with any of the MRI-derived parameters (Tables 3 and *SI Appendix*, Tables S7–S9).

Discussion

This study demonstrates that in utero MRI possesses the requisite sensitivity to detect abnormal fetal brain growth and maturation characteristics of fetuses exposed to ethanol early in gestation. This includes reduced cerebellar and brainstem volumes, and reduced diffusion anisotropy within associated white matter fascicles. Within the context of this animal model, although different BEC values were achieved by different animals, this variation was minor compared to the overall group difference in its effect on brain development. Importantly, these differences were only observable at the latest gestational age examined (G135). It is likely that brain regional volume differences were only found at this age because the fetal brain is too small, and hence size differences are too subtle, to identify at earlier gestational ages. Indices of water-diffusion anisotropy also exhibited highest sensitivity to alcohol exposure at G135. This is likely because white matter attains a stage of maturation that confers highest sensitivity of FA to differences in fiber tract structure. Thus, it is anticipated that the third trimester of gestation will be most sensitive for detecting alcohol-induced fetal brain growth abnormalities in human subjects. In addition to these group differences, dramatically enlarged lateral ventricles were found in 2 of the 14 ethanol-exposed fetuses (one G110 and one G135 fetus) (Fig. 1 *B* and *C*).

This study utilized a nonhuman primate model of FASD in which dams orally self-administered alcohol beginning prior to pregnancy and extending through the first 60 d of gestation. This pattern of drinking resembles women who drink alcohol but stop drinking upon pregnancy realization. Under such circumstances, MRI is a potentially powerful method that can complement biomarker-based studies, such as those used to characterize placental dysfunction (39, 40). Importantly, in utero MRI directed at detecting abnormal patterns of fetal CNS development is of specific relevance for characterizing risk for the emergence of subsequent behavioral impairments. Several previous studies have identified brain abnormalities in FASD, but these have been focused on subjects much later in life compared to this study. One advantage of using nonhuman primates as an animal model is the close match to humans in gestational term length relative to CNS development (21), which enables fetal MRI to be performed over a relevant stage of brain development for future applications. Additional advantages of this animal model include similarities to human drinking patterns, as detailed in ref. 20. For example, oral self-administration avoids confounds associated with gavage or intravenous administration, which induce maternal stress (41, 42). In contrast to studies of human subjects, the amount and timing of alcohol exposure is precisely known, and confounding factors, such as diet and exposure to other drugs of abuse, are controlled. An additional aspect of human maternal drinking behavior is that pregnant women are well conditioned to alcohol before conception. This is reflected in the present study as female monkeys were preconditioned to 1.5 g/kg alcohol for at least 30 d prior to conception (Fig. 1*A*).

Early-Gestation Fetal Ethanol Exposure Elicits Effects on Growth and Development of Brain Structures that Are Related to Motor Circuitry. The G135 cerebellum and brainstem were observed to be smaller in ethanol-exposed fetuses than controls (Fig. 2). Analysis of local shape differences revealed that the reduced cerebellar

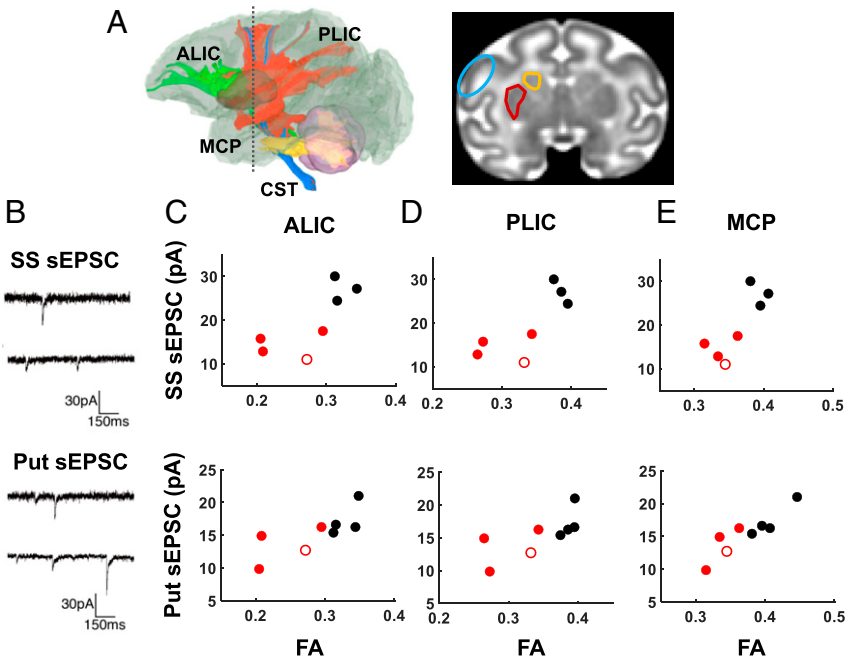

Fig. 4. Association between white matter FA and sEPSC amplitude. (*A*) Coronal views (*Right*) indicating the SS (blue) and dorsal striatal areas of the putamen (red) and caudate (orange) were obtained at the level depicted by the gray dashed line (*Left*). (*B*) Representative traces of sEPSC recorded from the SS (*Upper*) and putamen (put, *Lower*). In three of the four tracts that showed significant reductions in FA associated with fetal ethanol exposure (*A*, green, ALIC; red, PLIC; blue, CST; yellow, MCP), FA was found to correlate with EPSC amplitude measured in the SS (*C–E*, *Upper*) and the putamen (*C–E*, *Lower*). Black symbols: control fetuses; red symbols: ethanol-exposed fetuses; red open symbol: fetus F10289 who was exposed to 108 d of ethanol drinking.

volume resulted from smaller vermis, as well as bilaterally in the lateral lobule VI and Crus I. This finding closely parallels previous reports in human subjects (24, 25, 43–47), as well as animal model studies (48–53), demonstrating that fetal alcohol exposure is associated with smaller volume of the mature cerebellum. The reason for this brain region to be specifically vulnerable to the teratogenic effects of alcohol is not completely understood. It has been proposed that cerebellar development is preferentially sensitive to alcohol exposure during the protracted period of Purkinje cell dendritic arbor expansion (54, 55), which in primates, occurs during late gestation and continues into the postnatal period. However, systematic stereological comparisons of granule and Purkinje cell numbers in sheep that were exposed to similar levels of alcohol as in this study (53) have verified that exposure over a wide range of gestational periods can contribute to attenuated cerebellar growth. A refined interpretation is therefore that alcohol can interfere with development of cerebellar neural precursors early in gestation, perhaps as a consequence of epigenetic modifications (56; see ref. 57 for review), in addition to cellular morphological differentiation late in gestation (53). Experiments in rats, albeit utilizing a larger dose of alcohol (6.5 g/kg/d) further buttress the importance of early exposure, in which the total numbers of Purkinje and granule cells in the cerebellum of rat pups were significantly reduced relative to those of controls following an exposure period equivalent to human first two trimesters (49).

An additional finding of this study is that axonal tracts that support primary motor and somatosensory functions—such as the PLIC, CST, SCP, and MCP—exhibit reduced FA at G135 in association with the reduced volume of hindbrain structures. The observed difference in diffusion anisotropy is in agreement with findings that reduced FA was seen in various white matter tracts in FASD populations relative to controls, when measured postnatally (ranging from infancy to young adulthood) (26–36). Affected white matter systems include the CST (58), Cereb Ped (59), and internal capsule (29). However, the cellular processes that influence water diffusion in the G135 fetal brain differ from those at later stages of maturation because myelin formation is incomplete at G135. It is widely accepted that myelination is accompanied by an increase in water-diffusion anisotropy in developing white matter (60–63), but water-diffusion anisotropy also arises from unmyelinated axon bundles in the midgestation fetal brain (64, 65). Prior to myelination, FA increases as axons form fascicles and oligodendrocytes proliferate (18, 66). Hence, the reduced FA in axon fiber bundles of alcohol-exposed fetal brains observed here (Fig. 3) is consistent with deficits in

Table 3. Pearson's correlation coefficients and associated *P* values between white matter FA and sEPSC amplitudes recorded from the SS, putamen, and caudate

	SS sEPSC amplitude		Putamen sEPSC amplitude		Caudate sEPSC amplitude	
	r	*P*	*r*	*P*	*r*	*P*
CC	**0.77**	**0.044**	0.70	0.054	−0.15	0.75
ALIC	**0.76**	**0.049**	**0.77**	**0.024**	−0.34	0.45
PLIC	**0.77**	**0.041**	**0.72**	**0.045**	−0.30	0.51
AC	**0.79**	**0.035**	**0.72**	**0.042**	−0.33	0.47
Fornix	0.57	0.18	0.66	0.078	0.22	0.63
CST	**0.77**	**0.042**	0.41	0.31	0.033	0.94
SCP	**0.76**	**0.047**	0.69	0.058	−0.22	0.64
EC	0.63	0.13	0.68	0.062	−0.40	0.38
PTR	0.46	0.29	**0.91**	**0.0016**	−0.48	0.28
Cereb. Ped.	**0.78**	**0.037**	**0.82**	**0.013**	−0.49	0.26
MCP	**0.81**	**0.026**	**0.90**	**0.002**	−0.40	0.37

Correlation coefficient *r* and significance levels *P* were estimated using Pearson product moment correlation method, and an α of 0.05 (bold, $P < 0.05$).

maturation of white matter systems within the pyramidal tracts and other regions involved in somatosensory and motor circuitry. This close association between cerebellar and brainstem volumes with FA suggests a common vulnerability of the affected, functionally related brain regions.

The observed correlations between FA within the ALIC, PLIC, and MCP and excitatory, but not inhibitory, postsynaptic event amplitude in the SS and putamen suggest a functional significance to the anatomical effects of fetal alcohol observed in this study. Excitatory activity within the putamen is derived from neurons located outside of the striatum, whose axons must therefore contribute to the surrounding major fascicles, such as the ALIC and PLIC. Axons derived from nonlocal neurons similarly contribute to excitatory input within the SS. In contrast, inhibitory synaptic activity in the striatum and cortex is largely a product of local circuitry. Therefore, FA within white matter fascicles would be expected to correlate with excitatory postsynaptic activity more strongly than inhibitory activity. Electrophysiological studies of mice following fetal ethanol exposure have reported a similar regional pattern of sensitivity to that observed here. Specifically, neurons of the SS (37) and the dorsolateral striatum (equivalent to the rhesus putamen) but not dorsomedial striatum (equivalent to the rhesus caudate) (38) exhibit differences between ethanol-exposed and control offspring. However, in both of these studies, alterations to inhibitory synaptic signaling were found, which differs from the excitatory signaling effects observed here. It is possible that species differences, differences in the timing, dose, and route of ethanol exposure, as well as differences in the age in which the electrophysiological measurements were conducted, contribute to the divergent findings. Nevertheless, the regional distribution of anatomical effects observed here, within brain structures related to primary motor and somatosensory functions, is supported by the electrophysiological data, and leads to the prediction that primary motor functions supported by the affected regions would be deficient had the fetuses survived to postnatal life. Verification of this prediction will be sought in future studies.

It is noteworthy that the brain structural differences observed here are more specific to a functional domain than the brain-wide differences reported in other neuroimaging studies of FASD (67, 68). Several factors likely contribute to this. First, this study is focused on the fetal brain, and it is possible that some of the teratogenic effects of ethanol do not manifest until later stages of development. Second, the period of ethanol exposure was restricted to the equivalent of the human first trimester of pregnancy. It therefore is possible that the relatively early-developing elements of motor circuitry identified here undergo developmental processes that are specifically vulnerable to ethanol exposure early in gestation. Third, the ethanol dose, 1.5 g/kg/d of orally self-administered ethanol, is modest compared to other animal model studies that have reported more widespread brain effects (69, 70). Finally, considering the limited number of animals available for this study, more subtle structural effects could exist, but they are too subtle to be detected. In view of these factors, a conclusion from the present body of results is that the most easily detected (if not the only detectable) set of brain structural differences using in utero MRI is comprised by the motor-related gray matter structures and white matter fascicles identified here. Importantly, a prior study that utilized magnetic resonance microimaging of postmortem embryonic mouse brain tissue similarly identified the cerebellum volume as selectively vulnerable to early-gestation ethanol exposure (71). The microimaging technique can achieve higher spatial resolution than in vivo MRI methods. Therefore, the parallel findings between our studies support that the image resolution achievable with in utero MRI is sufficient to identify the same pattern of ethanol-induced structural differences as that identified with high-resolution 3D imaging methods. It is anticipated that in in utero MRI of human fetuses exposed to ethanol early in gestation will therefore be able to reveal reduced cerebellar volume, and abnormal maturation of associated white matter fibers, in the third trimester.

Experimental Design Considerations and Limitations. Due to relatively lengthy gestation, singleton pregnancies, and long induction period for alcohol self-administration, this study was limited to four to five fetuses per group per cohort. Thus, as mentioned above, it likely did not possess sufficient statistical power to detect the full spectrum of perturbations to the fetal brains at the exposure times, dosage, and gestational ages studied. It should also be noted that this study generated twice as many female fetuses as male fetuses (20). This imbalance in fetal sex distribution might be of importance because sexual dimorphism of brain volume reductions in FASD has been reported (72) wherein the magnitude of group differences (FASD vs. control) in volumes was greater among males than females. The unequal sex distribution attained in this study was not due to selective termination of male fetus pregnancies induced by ethanol, because all detected pregnancies were carried to the intended gestational age. Nevertheless, the fetal sex distribution in this study might reduce the magnitude of differences in brain volumes found in this study. A final limitation of the cross-sectional study design is that it was not possible to assess postnatal behavior in offspring animals. Given the vulnerability of brain regions involved in cerebellar and striatal circuitry, it is anticipated that animals generated with this model of FASD would exhibit motor impairments. It will be necessary to study additional animals with this experimental paradigm to test this prediction.

Conclusion

In utero MRI is a noninvasive method that enables fetal brain development to be monitored with high resolution. This capability provides an important tool for characterizing the anatomical bases of neurodevelopmental disorders at early stages of CNS development. In order to implement this new technique to assess development of human fetuses, it is necessary to understand the timing in which MRI methods are most sensitive to functionally relevant abnormalities. To address this, a nonhuman primate model of FASD was used here to specifically assess the implications of oral ethanol self-administration during early pregnancy. Abnormalities were observed in fetal cerebellar and brainstem growth and in the development of white matter fascicles related to sensory-motor function, at a time that corresponds to the third trimester of human gestation. These findings suggest that fetal MRI measurements performed later in pregnancy provide greater sensitivity to early-gestation ethanol exposure than MRI performed in midgestation. Based on the observed abnormalities, and the associated neurophysiological sequelae, it would be anticipated that the pattern of ethanol exposure produced in this study would result in offspring that exhibit impaired motor behavior, which is a prediction that can be addressed with future study of postnatal development in offspring degenerated with this experimental paradigm.

Materials and Methods

Rhesus Macaque FASD Model. All animal procedures were approved by the Oregon National Primate Research Center (ONPRC) and were conducted in full accordance with Public Health Service Policy in Humane Care and Use of Laboratory Animals. The generation of rhesus macaque fetuses used in this study is detailed in ref. 20. Female rhesus macaques that had completed at least one pregnancy were assigned to either an ethanol or a control group. All dams were single-housed in a temperature- and humidity-controlled room in which one side of their home cage was replaced by an operant panel that dispensed meals, water, and ethanol or maltose dextrin solution. Animals were induced to drink 1.5 g/kg per day of a 4% ethanol solution, or

a caloric equivalent maltose dextrin solution over a 120-d induction period, following previously established procedures (73, 74). Throughout the induction phase of the experiment, menses were monitored and plasma estradiol and progesterone levels were sampled. When a midcycle increase in estradiol level was detected, dams were paired with sires until a rapid decline of estradiol was observed (typically 3 to 5 d). The first day of gestation was defined as the day of peak plasma estradiol during the pairing period. In the ethanol group, each pregnant female maintained daily voluntary intake of 1.5 g/kg until G60, with the exception of one animal in the G135 cohort, which drank 1.5 g/kg daily for the first 109 d of gestation. BEC was measured once every 7 d, 90 min after initiating the daily drinking session, throughout the induction period, and the first 60 d of pregnancy (20, 73). All animals underwent awake ultrasound examination at G50 to confirm viable pregnancy.

Fetal MRI. To eliminate potential confounding effects of repeated exposure to isoflurane and ketamine (75, 76), a cross-sectional rather than longitudinal study design was employed. At G85, G110, and G135, pregnant females underwent anatomical and diffusion magnetic resonance examination of the fetal brain (Fig. 1*A*). Anesthesia was induced on dams with 10 mg/kg of ketamine and maintained with 1 to 1.5% isoflurane during MRI procedures. To facilitate later image reconstruction, multiple stacks were acquired through maternal axial, coronal, and sagittal planes for both T_2-weighted and diffusion magnetic resonance images. T_2-weighted images were acquired using half-Fourier acquisition single-shot turbo spin echo imaging at 0.5 mm × 0.5 mm × 1 mm with TR/TE = 1,200/102 ms. Between-slice motion was estimated collectively for all slices in all stacks using slice-intersection motion correction (77). All motion-scattered slices were then used to reconstruct a single 0.5-mm isotropic voxel resolution volume using deconvolution-based estimation (78) to remove the slice-profile blurring, and using slice-intersection bias correction (79) to account for between-slice signal-intensity differences.

Diffusion-weighted volumes including one "b0" and 20 diffusion-weighted volumes with b = 500 s/mm^2 were acquired using a diffusion-weighted, 2D spin-echo–based echoplanar imaging sequence. Raw diffusion data were acquired at 1.1-mm × 1.1-mm × 3-mm resolution (16). Between-slice motion was estimated within a unified diffusion model-based reconstruction framework (11), which also incorporated model-based deconvolution of slice-profile blurring, forming a single diffusion-weighted tensor estimate on a regular 0.75-mm voxel grid for final analysis. Diffusion tensor maps were used to calculate water diffusion FA.

ROI-Based Volume Analyses. Individual T_2-weighted volumes were nonlinearly registered to corresponding age-specific templates of rhesus macaque fetal brains (23) using ANTS SyN (symmetric normalization) (80). Then, the tissue labels delineated on the template images were propagated to individual spaces using the inverse of the transformation. Visual inspection was carried out to determine the robustness of transformation of the tissue labels to individual space. Only 2 (fetus 10283 in the G110 ethanol group and fetus 10290 in the G135 ethanol group) of 27 cases required manual editing due to their significant structural and morphological deviation from the template (Fig. 1 *B* and *C*). Absolute volumes for each structure featured in the atlases were then determined for each individual fetal brain.

Tensor-Based Morphometry. Tensor-based morphometry analysis was used to localize regions of shape differences between control and ethanol-exposed fetal brains, based on deformation fields that transform points in a template volume to equivalent points in an individual volume. This required the generation of three study-specific T_2-weighted templates, constructed from four control fetuses and four alcohol-exposed fetuses for the three cohorts using ANTS "buildtemplateparallel.sh" script with "Greedy SyN" as diffeomorphic registration model and cross-correlation as similarity metric (81). The two fetuses with enlarged lateral ventricles (Fig. 1 *B* and *C*) (one from the G110 cohort and one from the G135 cohort) were excluded from template construction due to their drastic deformation from normal brain morphology. Next, each T_2-weighted volume was nonlinearly registered to the study-specific template using "antsRegistrationSyN.sh" (81, 82), during which a warp field was generated. To examine local expansion or contraction of individual brains relative to corresponding template volume, logarithms of Jacobian determinant maps were derived from the warp fields using ANTs "CreateJacobianDeterminantImage." A positive value of the resulting map means the template is expanding to match the individual volume, whereas a negative value means the template is contracting to match the individual volume. A nonparametric two-sample unpaired *t* test with two contrasts, Control–Ethanol and Ethanol–Control, was carried out using the "randomize" function (83) with the threshold-free cluster enhanced (TFCE) option (84) included in the FSL library (85). Clusters with uncorrected $P \leq 0.05$ and sizes ≥1,000 voxels (125 mm^3) were overlaid onto each study-specific template.

White Matter Characterization. Similar to volumetric estimation, FA maps of individual fetal brains were registered to age-specific FA templates of rhesus macaque fetal brains (23). White matter ROIs featured in the atlas were then propagated back to individual FA maps and FA values were averaged within each ROI for each fetal brain. White matter tractography was performed on one G135 control fetal brain using a deterministic diffusion fiber tracking method (86) (http://dsi-studio.labsolver.org/), with defined white matter ROIs as seeds, an FA threshold of 0.1, an angular threshold of 30°, a step size of 0.38 mm, seed minimum/maximum lengths of 1.00 mm/100.00 mm, respectively, and a trilinear method for direction interpolation (Fig. 4*A*).

A tract-based spatial statistics (TBSS) (87) approach was used to compare white matter FA of the control and alcohol-exposed fetuses. In brief, 1) FA maps of each fetal brain were registered to the age-specific FA templates generated in previous steps, giving a warped FA map in the template space. 2) A mean FA map was then derived by averaging all of the warped FA maps in each cohort, from which a skeleton was generated using "tbss_skeleton" included in the FSL library. 3) The skeleton was manually edited to remove cortical gray matter regions, which have relatively high FA, to yield a white matter skeleton. 4) The white matter skeleton was further threshold at a value of 0.2 to generate a binary skeleton mask and a distance map in the template space. Individual warped FA maps were also skeletonized by projecting white matter FA values to the white matter skeleton. These steps were done using a single command "tbss_4_prestats" in the FSL library. 5) Similar to tensor-based morphometry, nonparametric two-sample unpaired *t* test with two contrasts, Control–Ethanol and Ethanol–Control, was carried out using the FSL "randomize" method with TFCE as described above.

Statistical Analyses of Brain Region Volumes and Average FA Values. All statistical analyses were performed using the R software platform (http://www.R-project.org). Analyses of brain region volumes and diffusion anisotropy were performed to test the hypothesis that brain region volumes are smaller, and FA values are lower, in the ethanol-exposed fetuses compared to those of gestation age-matched control fetuses. For each of the three gestational ages examined in this study, six common brain regions were analyzed (88). These are the cortical plate, the developing white matter (termed subplate and intermediate zone at G85), the striatum, the thalamus, the brainstem, and the cerebellum. In addition, FA within 8 white matter ROIs were analyzed in the G110 cohort and 11 white matter ROIs in the G135 cohort (23). Within each of the six groups (ethanol-exposed and control groups at three gestational ages), the distributions of all brain region volumes and all FA values were found to be normally distributed (Shapiro–Wilk test, $P > 0.05$). Two-sample, one-tailed *t* tests, with equal ($P > 0.05$ from Bartlett's test) or unequal ($P \leq 0.05$ from Bartlett test) variance, were used to compare brain region volumes and FA values between the control and ethanol-exposed groups at each gestational age. Within each gestational age, multiple hypotheses were tested. A total of 6 hypotheses were tested for G85 fetuses, 14 hypotheses were tested for G110 fetuses, and 17 hypotheses were tested for the G135 fetuses. Therefore, *P* values from *t* tests were corrected for false-discovery rate using a Benjamini–Hochberg (89) procedure implemented in R using the function "p.adjust," with the option "BH" specified. Corrected $P \leq 0.05$ are considered significant in this study.

Whole-Cell Patch-Clamp Electrophysiology. All fetuses were delivered via Cesarean section immediately following fetal MRI examination. Upon delivery, fetuses were killed with an overdose of pentobarbital, and the brains were perfused with ice-cold artificial cerebrospinal fluid (aCSF) (90) through the carotid artery. Brains of all except for two of the G135 fetuses (one control and one ethanol-exposed animal) (Table 2) (20) were removed and immersed in ice-cold aCSF for subsequent electrophysiological measurements. The left hemispheres were blocked into roughly 4-mm-thick coronal slabs. The primary SS and the dorsal striatum were separated from the remaining tissue and further sectioned for electrophysiolgical analysis, as previously published (90, 91). Briefly, coronal sections (250 μm) were obtained in ice-cold cutting solution and equilibrated for 1 h at 33 °C in aCSF. Next, slices were transferred to a recording chamber fixed to the stage of an upright microscope (Axioskop2, Zeiss), stabilized by an overlying platinum ring, and continuously perfused with solution maintained within a temperature range of 28 to 32 °C (Automatic temperature Controller, Warner Instruments). Pyramidal neurons in the SS and medium spiny neurons within the dorsal

striatum were identified under infrared optics using a 40× water-immersion objective. Although the lack of cytoarchitectural differentiation at G135 precluded determination of cortical layers within the SS, recordings were performed from the deepest third of the cortical plate in putative layers V-VI. Recording patch pipettes with outer diameter of 1.5 mm and inner diameter of 0.86 mm (Sutter Instruments) were filled with either K-gluconate– or CsCl-based internal solutions. Recordings were made on 6 to 10 cells per region for each animal using a Multiclamp 600B amplifier (Molecular Devices). Whole-cell currents were filtered at 2 kHz, digitized at 10 kHz using Clampex v10.5, and analyzed with MiniAnalysis (Synaptosoft v6.0.7). The initial detection of sEPSCs and sIPSCs was performed with amplitude and area as a threshold (10 pA and either 20fc or 50fc for sEPSC or sIPSC, respectively). This initial amplitude threshold was changed for some recordings dependent on the noise level of the recording. False events were rejected (i.e., those that did not show fast rising phases) upon further visual analysis. Series resistance were monitored at regular intervals throughout each recording and data were discarded if resistance was greater than 25 mΩ or changed by more than 15% during a given experiment.

Data Availability. MRI-derived parameters and electrophysiological results obtained as part of this study are available through the Monkey Alcohol Tissue Research Resource https://gleek.ecs.baylor.edu/static/publication_data/FAS_Cohort_MRI_Ephys_Data_Wang_et_at_2020.xlsx. Template T2-weighted images and FA maps, in addition to the labelmaps used to quantify image parameters, are available at https://www.nitrc.org/projects/fetalmacaatlas (92).

ACKNOWLEDGMENTS. This research was supported by NIH Grant R01AA021981. Salary support was additionally received from P51OD011092 (V.C.C.C., K.A.G., and C.D.K.), R01NS055064 (C.S.), and R01AA024757 (M.M.F.).

1. T. E. Moore, K. R. Gagnier, "Fetal alcohol syndrome" in *The Corsini Encyclopedia of Psychology*, I. B. Weiner, W. E. Craighead, Eds. (John Wiley & Sons, Inc., 2010), pp. 657–659.
2. P. A. May *et al*., Prevalence of fetal alcohol spectrum disorders in 4 US communities. *JAMA* **319**, 474–482 (2018).
3. S. Popova, S. Lange, C. Probst, G. Gmel, J. Rehm, Global prevalence of alcohol use and binge drinking during pregnancy, and fetal alcohol spectrum disorder. *Biochem. Cell Biol.* **96**, 237–240 (2018).
4. S. Lange *et al*., Global prevalence of fetal alcohol spectrum disorder among children and youth: A systematic review and meta-analysis. *JAMA Pediatr.* **171**, 948–956 (2017).
5. L. B. Finer, M. R. Zolna, Declines in unintended pregnancy in the United States, 2008–2011. *N. Engl. J. Med.* **374**, 843–852 (2016).
6. CDC, *Behavioral Risk Factor Surveillance System User's Guide* (US Centers for Disease Control and Prevention, Atlanta, GA, 2019).
7. C. H. Denny, C. S. Acero, T. S. Naimi, S. Y. Kim, Consumption of alcohol beverages and binge drinking among pregnant women aged 18–44 years–United States, 2015–2017. *MMWR Morb. Mortal. Wkly. Rep.* **68**, 365–368 (2019).
8. P. Yazdani, M. Motz, G. Koren, Estimating the neurocognitive effects of an early intervention program for children with prenatal alcohol exposure. *Can. J. Clin. Pharmacol.* **16**, e453–e459 (2009).
9. A. P. Streissguth *et al*., Risk factors for adverse life outcomes in fetal alcohol syndrome and fetal alcohol effects. *J. Dev. Behav. Pediatr.* **25**, 228–238 (2004).
10. C. Studholme, Mapping fetal brain development in utero using magnetic resonance imaging: The Big Bang of brain mapping. *Annu. Rev. Biomed. Eng.* **13**, 345–368 (2011).
11. M. Fogtmann *et al*., A unified approach to diffusion direction sensitive slice registration and 3-D DTI reconstruction from moving fetal brain anatomy. *IEEE Trans. Med. Imaging* **33**, 272–289 (2014).
12. S. Jiang *et al*., In-utero three dimension high resolution fetal brain diffusion tensor imaging. *Med. Image Comput. Comput. Assist. Interv.* **10**, 18–26 (2007).
13. J. A. Scott *et al*., Growth trajectories of the human fetal brain tissues estimated from 3D reconstructed in utero MRI. *Int. J. Dev. Neurosci.* **29**, 529–536 (2011).
14. K. M. Adams Waldorf *et al*., Congenital Zika virus infection as a silent pathology with loss of neurogenic output in the fetal brain. *Nat. Med.* **24**, 368–374 (2018).
15. N. N. Andescavage *et al*., Complex trajectories of brain development in the healthy human fetus. *Cereb. Cortex* **27**, 5274–5283 (2017).
16. X. Wang *et al*., Folding, but not surface area expansion, is associated with cellular morphological maturation in the fetal cerebral cortex. *J. Neurosci.* **37**, 1971–1983 (2017).
17. A. J. Hirsch *et al*., Zika virus infection in pregnant rhesus macaques causes placental dysfunction and immunopathology. *Nat. Commun.* **9**, 263 (2018).
18. E. Zanin *et al*., White matter maturation of normal human fetal brain. An in vivo diffusion tensor tractography study. *Brain Behav.* **1**, 95–108 (2011).
19. S. Khan *et al*., Fetal brain growth portrayed by a spatiotemporal diffusion tensor MRI atlas computed from in utero images. *Neuroimage* **185**, 593–608 (2019).
20. V. A. Jimenez *et al*., Detecting neurodevelopmental effects of early-gestation ethanol exposure: A nonhuman primate model of ethanol drinking during pregnancy. *Alcohol. Clin. Exp. Res.* **43**, 250–261 (2019).
21. A. D. Workman, C. J. Charvet, B. Clancy, R. B. Darlington, B. L. Finlay, Modeling transformations of neurodevelopmental sequences across mammalian species. *J. Neurosci.* **33**, 7368–7383 (2013).
22. J. O. Lo *et al*., Novel detection of placental insufficiency by magnetic resonance imaging in the nonhuman primate. *Reprod. Sci.* **25**, 64–73 (2018).
23. Z. Liu *et al*., Anatomical and diffusion MRI brain atlases of the fetal rhesus macaque brain at 85, 110 and 135 days gestation. *Neuroimage* **206**, 116310 (2020).
24. E. R. Sowell *et al*., Abnormal development of the cerebellar vermis in children prenatally exposed to alcohol: Size reduction in lobules I-V. *Alcohol. Clin. Exp. Res.* **20**, 31–34 (1996).
25. E. D. O'Hare *et al*., Mapping cerebellar vermal morphology and cognitive correlates in prenatal alcohol exposure. *Neuroreport* **16**, 1285–1290 (2005).
26. X. Ma *et al*., Evaluation of corpus callosum anisotropy in young adults with fetal alcohol syndrome according to diffusion tensor imaging. *Alcohol. Clin. Exp. Res.* **29**, 1214–1222 (2005).
27. J. R. Wozniak *et al*., Diffusion tensor imaging in children with fetal alcohol spectrum disorders. *Alcohol. Clin. Exp. Res.* **30**, 1799–1806 (2006).
28. C. Lebel *et al*., Brain diffusion abnormalities in children with fetal alcohol spectrum disorder. *Alcohol. Clin. Exp. Res.* **32**, 1732–1740 (2008).
29. E. R. Sowell *et al*., Mapping white matter integrity and neurobehavioral correlates in children with fetal alcohol spectrum disorders. *J. Neurosci.* **28**, 1313–1319 (2008).
30. S. L. Fryer *et al*., Characterization of white matter microstructure in fetal alcohol spectrum disorders. *Alcohol. Clin. Exp. Res.* **33**, 514–521 (2009).
31. S. E. Parnell *et al*., Magnetic resonance microscopy defines ethanol-induced brain abnormalities in prenatal mice: Effects of acute insult on gestational day 8. *Alcohol. Clin. Exp. Res.* **33**, 1001–1011 (2009).
32. J. R. Wozniak *et al*., Microstructural corpus callosum anomalies in children with prenatal alcohol exposure: An extension of previous diffusion tensor imaging findings. *Alcohol. Clin. Exp. Res.* **33**, 1825–1835 (2009).
33. K. A. Donald *et al*., A study of the effects of prenatal alcohol exposure on white matter microstructural integrity at birth. *Acta Neuropsychiatr.* **27**, 197–205 (2015).
34. J. Fan *et al*., White matter integrity of the cerebellar peduncles as a mediator of effects of prenatal alcohol exposure on eyeblink conditioning. *Hum. Brain Mapp.* **36**, 2470–2482 (2015).
35. J. Fan *et al*., White matter deficits mediate effects of prenatal alcohol exposure on cognitive development in childhood. *Hum. Brain Mapp.* **37**, 2943–2958 (2016).
36. P. A. Taylor *et al*., A DTI-based tractography study of effects on brain structure associated with prenatal alcohol exposure in newborns. *Hum. Brain Mapp.* **36**, 170–186 (2015).
37. L. C. Delatour, P. W. Yeh, H. H. Yeh, Ethanol exposure in utero disrupts radial migration and pyramidal cell development in the somatosensory cortex. *Cereb. Cortex* **29**, 2125–2139 (2019).
38. V. C. Cuzon Carlson, C. M. Gremel, D. M. Lovinger, Gestational alcohol exposure disrupts cognitive function and striatal circuits in adult offspring. *Nat. Commun.*, in press.
39. A. M. Tseng *et al*.; Collaborative Initiative on Fetal Alcohol Spectrum Disorders, Maternal circulating miRNAs that predict infant FASD outcomes influence placental maturation. *Life Sci. Alliance* **2**, e201800252 (2019).
40. J. O. Lo *et al*., First trimester alcohol exposure alters placental perfusion and fetal oxygen availability affecting fetal growth and development in a non-human primate model. *Am. J. Obstet. Gynecol.* **216**, 302.e1–302.e8 (2017).
41. K. S. Hougaard, A. M. Hansen, Enhancement of developmental toxicity effects of chemicals by gestational stress. A review. *Neurotoxicol. Teratol.* **29**, 425–445 (2007).
42. A. S. Clarke, M. L. Schneider, Prenatal stress has long-term effects on behavioral responses to stress in juvenile rhesus monkeys. *Dev. Psychobiol.* **26**, 293–304 (1993).
43. S. J. Astley *et al*., Magnetic resonance imaging outcomes from a comprehensive magnetic resonance study of children with fetal alcohol spectrum disorders. *Alcohol. Clin. Exp. Res.* **33**, 1671–1689 (2009).
44. R. Riikonen, I. Salonen, K. Partanen, S. Verho, Brain perfusion SPECT and MRI in foetal alcohol syndrome. *Dev. Med. Child Neurol.* **41**, 652–659 (1999).
45. S. L. Archibald *et al*., Brain dysmorphology in individuals with severe prenatal alcohol exposure. *Dev. Med. Child Neurol.* **43**, 148–154 (2001).
46. I. Autti-Rämö *et al*., MRI findings in children with school problems who had been exposed prenatally to alcohol. *Dev. Med. Child Neurol.* **44**, 98–106 (2002).
47. V. A. Cardenas *et al*., Automated cerebellar segmentation: Validation and application to detect smaller volumes in children prenatally exposed to alcohol. *Neuroimage Clin.* **4**, 295–301 (2014).
48. C. Bauer-Moffett, J. Altman, The effect of ethanol chronically administered to preweanling rats on cerebellar development: A morphological study. *Brain Res.* **119**, 249–268 (1977).
49. S. E. Maier, J. R. West, Regional differences in cell loss associated with binge-like alcohol exposure during the first two trimesters equivalent in the rat. *Alcohol* **23**, 49–57 (2001).
50. J. Ramadoss, E. R. Lunde, W. J. Chen, J. R. West, T. A. Cudd, Temporal vulnerability of fetal cerebellar Purkinje cells to chronic binge alcohol exposure: Ovine model. *Alcohol. Clin. Exp. Res.* **31**, 1738–1745 (2007).
51. J. Ramadoss, E. R. Lunde, K. B. Piña, W. J. Chen, T. A. Cudd, All three trimester binge alcohol exposure causes fetal cerebellar Purkinje cell loss in the presence of maternal hypercapnea, acidemia, and normoxemia: Ovine model. *Alcohol. Clin. Exp. Res.* **31**, 1252–1258 (2007).

52. S. E. Parnell, H. E. Holloway, L. K. Baker, M. A. Styner, K. K. Sulik, Dysmorphogenic effects of first trimester-equivalent ethanol exposure in mice: A magnetic resonance microscopy-based study. *Alcohol. Clin. Exp. Res.* **38**, 2008–2014 (2014).
53. O. B. Sawant *et al*., Different patterns of regional Purkinje cell loss in the cerebellar vermis as a function of the timing of prenatal ethanol exposure in an ovine model. *Neurotoxicol. Teratol.* **35**, 7–13 (2013).
54. C. R. Goodlett, K. M. Hamre, J. R. West, Regional differences in the timing of dendritic outgrowth of Purkinje cells in the vermal cerebellum demonstrated by MAP2 immunocytochemistry. *Brain Res. Dev. Brain Res.* **53**, 131–134 (1990).
55. C. R. Goodlett, B. L. Marcussen, J. R. West, A single day of alcohol exposure during the brain growth spurt induces brain weight restriction and cerebellar Purkinje cell loss. *Alcohol* **7**, 107–114 (1990).
56. W. Guo *et al*., Alcohol exposure decreases CREB binding protein expression and histone acetylation in the developing cerebellum. *PLoS One* **6**, e19351 (2011).
57. M. Ungerer, J. Knezovich, M. Ramsay, In utero alcohol exposure, epigenetic changes, and their consequences. *Alcohol Res.* **35**, 37–46 (2013).
58. A. Paolozza, S. Treit, C. Beaulieu, J. N. Reynolds, Diffusion tensor imaging of white matter and correlates to eye movement control and psychometric testing in children with prenatal alcohol exposure. *Hum. Brain Mapp.* **38**, 444–456 (2017).
59. B. S. Spottiswoode *et al*., Diffusion tensor imaging of the cerebellum and eyeblink conditioning in fetal alcohol spectrum disorder. *Alcohol. Clin. Exp. Res.* **35**, 2174–2183 (2011).
60. P. Mukherjee *et al*., Normal brain maturation during childhood: Developmental trends characterized with diffusion-tensor MR imaging. *Radiology* **221**, 349–358 (2001).
61. J. J. Neil *et al*., Normal brain in human newborns: Apparent diffusion coefficient and diffusion anisotropy measured by using diffusion tensor MR imaging. *Radiology* **209**, 57–66 (1998).
62. C. Lebel, C. Beaulieu, Longitudinal development of human brain wiring continues from childhood into adulthood. *J. Neurosci.* **31**, 10937–10947 (2011).
63. X. Ou *et al*., Gestational age at birth and brain white matter development in term-born infants and children. *AJNR Am. J. Neuroradiol.* **38**, 2373–2379 (2017).
64. C. Mitter, D. Prayer, P. C. Brugger, M. Weber, G. Kasprian, In vivo tractography of fetal association fibers. *PLoS One* **10**, e0119536 (2015).
65. G. Kasprian *et al*., In utero tractography of fetal white matter development. *Neuroimage* **43**, 213–224 (2008).
66. J. Dubois *et al*., The early development of brain white matter: A review of imaging studies in fetuses, newborns and infants. *Neuroscience* **276**, 48–71 (2014).
67. K. A. Donald *et al*., Neuroimaging effects of prenatal alcohol exposure on the developing human brain: A magnetic resonance imaging review. *Acta Neuropsychiatr.* **27**, 251–269 (2015).
68. V. T. Nguyen *et al*., Radiological studies of fetal alcohol spectrum disorders in humans and animal models: An updated comprehensive review. *Magn. Reson. Imaging* **43**, 10–26 (2017).
69. S. K. O'Leary-Moore *et al*., Magnetic resonance microscopy-based analyses of the brains of normal and ethanol-exposed fetal mice. *Birth Defects Res. A Clin. Mol. Teratol.* **88**, 953–964 (2010).
70. L. A. Leigland, M. M. Ford, J. P. Lerch, C. D. Kroenke, The influence of fetal ethanol exposure on subsequent development of the cerebral cortex as revealed by magnetic resonance imaging. *Alcohol. Clin. Exp. Res.* **37**, 924–932 (2013).
71. S. E. Parnell *et al*., Magnetic resonance microscopy-based analyses of the neuroanatomical effects of gestational day 9 ethanol exposure in mice. *Neurotoxicol. Teratol.* **39**, 77–83 (2013).
72. S. Treit *et al*., Sexual dimorphism of volume reduction but not cognitive deficit in fetal alcohol spectrum disorders: A combined diffusion tensor imaging, cortical thickness and brain volume study. *Neuroimage Clin.* **15**, 284–297 (2017).
73. K. A. Grant *et al*., Drinking typography established by scheduled induction predicts chronic heavy drinking in a monkey model of ethanol self-administration. *Alcohol. Clin. Exp. Res.* **32**, 1824–1838 (2008).
74. J. A. Vivian *et al*., Induction and maintenance of ethanol self-administration in cynomolgus monkeys (Macaca fascicularis): Long-term characterization of sex and individual differences. *Alcohol. Clin. Exp. Res.* **25**, 1087–1097 (2001).
75. A. M. Brambrink *et al*., Isoflurane-induced apoptosis of oligodendrocytes in the neonatal primate brain. *Ann. Neurol.* **72**, 525–535 (2012).
76. A. M. Brambrink *et al*., Ketamine-induced neuroapoptosis in the fetal and neonatal rhesus macaque brain. *Anesthesiology* **116**, 372–384 (2012).
77. K. Kim *et al*., Intersection based motion correction of multislice MRI for 3-D in utero fetal brain image formation. *IEEE Trans. Med. Imaging* **29**, 146–158 (2010).
78. M. Fogtmann, S. Seshamani, K. Kim, T. Chapman, C. Studholme, "A unified approach for motion estimation and super resolution reconstruction from structural Magnetic Resonance imaging on moving subjects" in *MICCAI Workshop on Perinatal and Paediatric Imaging* (Nice, 2012).
79. K. Kim *et al*., Bias field inconsistency correction of motion-scattered multislice MRI for improved 3D image reconstruction. *IEEE Trans. Med. Imaging* **30**, 1704–1712 (2011).
80. B. B. Avants, C. L. Epstein, M. Grossman, J. C. Gee, Symmetric diffeomorphic image registration with cross-correlation: Evaluating automated labeling of elderly and neurodegenerative brain. *Med. Image Anal.* **12**, 26–41 (2008).
81. B. B. Avants *et al*., A reproducible evaluation of ANTs similarity metric performance in brain image registration. *Neuroimage* **54**, 2033–2044 (2011).
82. N. J. Tustison, B. B. Avants, Explicit B-spline regularization in diffeomorphic image registration. *Front. Neuroinform.* **7**, 39 (2013).
83. A. M. Winkler, G. R. Ridgway, M. A. Webster, S. M. Smith, T. E. Nichols, Permutation inference for the general linear model. *Neuroimage* **92**, 381–397 (2014).
84. S. M. Smith, T. E. Nichols, Threshold-free cluster enhancement: Addressing problems of smoothing, threshold dependence and localisation in cluster inference. *Neuroimage* **44**, 83–98 (2009).
85. M. Jenkinson, C. F. Beckmann, T. E. Behrens, M. W. Woolrich, S. M. Smith, FSL. *Neuroimage* **62**, 782–790 (2012).
86. F. C. Yeh, T. D. Verstynen, Y. Wang, J. C. Fernández-Miranda, W. Y. Tseng, Deterministic diffusion fiber tracking improved by quantitative anisotropy. *PLoS One* **8**, e80713 (2013).
87. S. M. Smith *et al*., Tract-based spatial statistics: Voxelwise analysis of multi-subject diffusion data. *Neuroimage* **31**, 1487–1505 (2006).
88. Z. Liu *et al*., The effects of breastfeeding versus formula-feeding on cerebral cortex maturation in infant rhesus macaques. *Neuroimage* **184**, 372–385 (2019).
89. Y. Benjamini, Y. Hochberg, Controlling the false discovery rate—A practical and powerful approach to multiple testing. *J. R. Stat. Soc. B* **57**, 289–300 (1995).
90. V. C. Cuzon Carlson *et al*., Synaptic and morphological neuroadaptations in the putamen associated with long-term, relapsing alcohol drinking in primates. *Neuropsychopharmacology* **36**, 2513–2528 (2011).
91. V. C. Cuzon Carlson, K. A. Grant, D. M. Lovinger, Synaptic adaptations to chronic ethanol intake in male rhesus monkey dorsal striatum depend on age of drinking onset. *Neuropharmacology* **131**, 128–142 (2018).
92. NeuroImaging Tools & Resources Collaboratory, ONPRC Fetal Macaque Brain Atlas. https://www.nitrc.org/projects/fetalmacaatlas. Accessed 7 April 2020.